Absolute Value Layered ACO-OFDM for Intensity-Modulated Optical Wireless Channels

Ruowen Bai, *Graduate Student Member, IEEE*, and Steve Hranilovic, *Senior Member, IEEE*

***Abstract*— Enhanced unipolar orthogonal frequency division multiplexing (eU-OFDM) and layered asymmetrically clipped optical OFDM (LACO-OFDM) are spectrally efficient modulation techniques for intensity modulated systems which layer multiple non-negative signals. In this paper, we propose *absolute value layered asymmetrically clipped optical OFDM* (ALACO-OFDM), which further improves the spectral efficiency while using a smaller number of layers and no explicit direct current (DC) bias. In ALACO-OFDM, asymmetrically clipped optical OFDM (ACO-OFDM) signals are sent at the first L layers and absolute value optical OFDM (AVO-OFDM) is used for the remaining subcarriers and transmitted simultaneously. Analysis indicates that ALACO- achieves higher spectral efficiency than eU- or LACO-OFDM while using a smaller number of layers. Bounds on achievable information rates of ALACO-OFDM and related layered ACO-OFDM techniques are also developed. Two optical power allocation schemes over the layers of ALACO-OFDM are developed with the objective of optimizing uncoded transmission performance and the achievable information rate respectively. Additionally, a theoretical bound on the uncoded BER of ALACO-OFDM is derived. Monte Carlo simulation results indicate ALACO-OFDM with the optimum power allocation achieves significant uncoded BER performance gains compared to its counterparts at the same spectral efficiency while having a smaller peak-to-average power ratio.**

***Index Terms*— Orthogonal frequency division multiplexing (OFDM), LACO-OFDM, eU-OFDM, AAO-OFDM, intensity modulation with direct detection (IM/DD).**

I. Introduction

WHILE a majority of wireless communications systems operate in the radio bands, optical wireless communications (OWC) has recently emerged as an attractive complementary link due to the ubiquity of solid-state illumination and the availability of large amounts of unregulated spectrum [1], [2]. Data are conveyed by modulating the instantaneous optical intensity (i.e., intensity modulation (IM)) and detecting the received signal power using a photodiode (i.e., direct detection (DD)). Such IM/DD links impose constraints on the non-negativity of all emitted signals and constrain the average amplitude [1]–[3].

Manuscript received November 22, 2019; revised April 7, 2020 and June 3, 2020; accepted July 15, 2020. Date of publication July 21, 2020; date of current version November 18, 2020. This work was supported by the Natural Sciences and Engineering Reseach Council of Canada. This article was presented in part at the IEEE International Conference on Communications (ICC 2019), 2019. The associate editor coordinating the review of this article and approving it for publication was G.-C. Yang. *(Corresponding author: Steve Hranilovic.)*

The authors are with the Department of Electrical and Computer Engineering, McMaster University, Hamilton, ON L8S 4L8, Canada (e-mail: bair4@mcmaster.ca; hranilovic@mcmaster.ca).

Color versions of one or more of the figures in this article are available online at http://ieeexplore.ieee.org.

Digital Object Identifier 10.1109/TCOMM.2020.3010986

Many of these optical wireless channels, especially those that arise due to visible light communications (VLC), are bandwidth limited. In this context, spectrally efficient orthogonal frequency division multiplexing (OFDM) has been investigated for OWC to enhance the data rate while satisfying IM/DD amplitude constraints. To generate a real-value time-domain signal, Hermitian symmetry in the spectrum is required [4]. However, many approaches exist to ensure amplitude non-negativity. In direct current (DC) biased optical OFDM (DCO-OFDM) a conventional OFDM signal is biased to ensure non-negativity. Although this preserves its high spectral efficiency, the addition of a large DC bias makes this approach power inefficient [4]. Approaches such as asymmetrically clipped optical OFDM (ACO-OFDM) [5] and unipolar OFDM (U-OFDM) [6] are more power efficient and ensure amplitude non-negativity at a cost of half of the spectral efficiency. To address this spectral efficiency loss, enhanced U-OFDM (eU-OFDM) superimposing multiple streams of U-OFDM [6], and layered ACO-OFDM (LACO-OFDM), superimposing multiple layers of ACO-OFDM [7]–[11], have been proposed. In general, both approaches work by layering a number of non-negative signals and performing successive detection at the receiver. In theory, the spectral efficiency of eU- and LACO-OFDM approaches that of DCO-OFDM as the number of layers or streams increases. However, using a large number of layers incurs high computational complexity and latency in the demodulator. Recently, asymmetrically clipped absolute value optical OFDM (AAO-OFDM) [3] has been proposed to enhance the spectral efficiency, in which no explicit DC bias is required. Although AAO-OFDM has only two streams, the spectral efficiency is still 0.5 bits/channel use smaller than that of DCO-OFDM.

In this work we present *absolute value layered ACO-OFDM* (ALACO-OFDM), which has a spectral efficiency approaching that of DCO-OFDM while preserving power efficiency [12]. Different from dual-stream AAO-OFDM [3], in ALACO-OFDM, ACO-OFDM signals are sent in the first L layers and absolute value optical OFDM (AVO-OFDM) [3] is used over the remaining subcarriers. These streams are superimposed in the time domain and transmitted simultaneously with no explicit DC bias. Thus, AAO-OFDM in [3] is a special case of ALACO-OFDM with $L = 1$. At the receiver, the L layers of ACO-OFDM symbols are first demodulated layer-by-layer as in LACO-OFDM [9] and then the AVO-OFDM symbols are demodulated with the aid of sign information carried in the first layer. In order to design an ALACO-OFDM system, two optimal power allocations over the layers are derived which optimize uncoded bit error rate (BER) and information

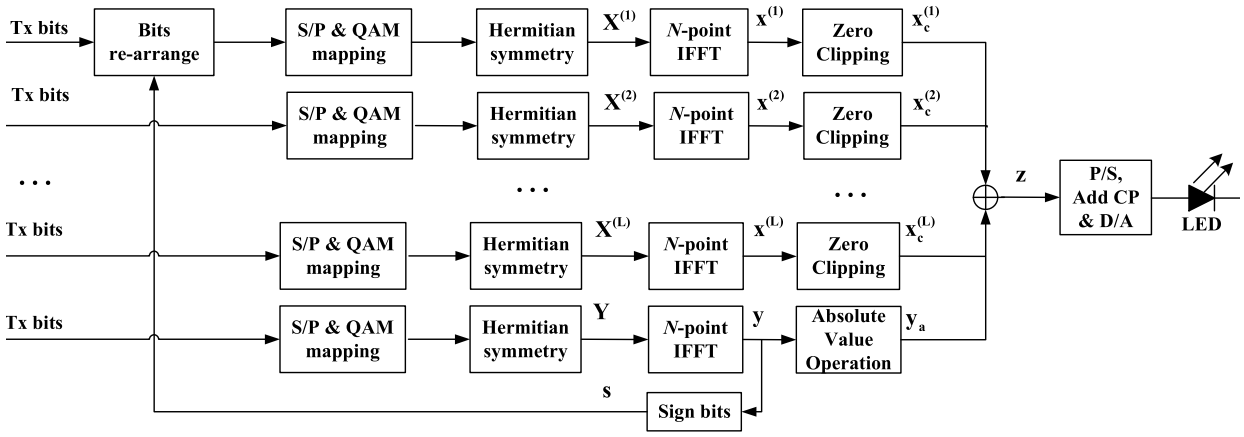

Fig. 1. Transmitter design block diagram for ALACO-OFDM.

rate, respectively. Our analysis indicates that for the same spectral efficiency, ALACO-OFDM requires fewer layers, and is less complex than LACO-OFDM in terms of the number of real-valued multiplication operations and real-valued addition operations. Additionally, ALACO-OFDM achieves higher information rate than ACO-, AAO- and LACO-OFDM at moderate to high signal-to-noise ratios (SNRs). Furthermore, a theoretical bound on the BER of ALACO-OFDM is derived, which is close to the simulation results in high SNR regime. A BER performance comparison indicates uncoded ALACO-OFDM achieves significant gains over AAO-, LACO- and eU-OFDM. In terms of peak-to-average power ratio (PAPR), ALACO-OFDM is also shown to have a lower PAPR than ACO-, AAO-, LACO- or eU-OFDM.

Section II defines the ALACO-OFDM transmitter and receiver. The spectral efficiency and complexity of the ALACO-OFDM are analyzed and compared to its counterparts in Sec. III. Two optimal optical power allocation schemes are designed with respect to uncoded BER and achievable information rate in Sec. IV. The BER and PAPR performance of ALACO-OFDM are presented and compared to its counterparts in Sec. V. Finally, conclusions are drawn in Sec. VI.

II. Definition of ALACO-OFDM

A. Transmitter

The transmitter block diagram for an ALACO-OFDM based IM/DD system with N subcarriers is shown in Fig. 1, where N is assumed to be a power of 2. The ALACO-OFDM signal consists of L layers of ACO-OFDM [9] and a single layer of AVO-OFDM [3].

Transmitted bits are serial-to-parallel (S/P) converted and mapped to quadrature amplitude modulation (QAM) constellation symbols. To obtain a real-valued time-domain signal, Hermitian symmetry is imposed on the N subcarriers, where $X_k = X^*_{N-k}$, and X_0 and $X_{N/2}$ are set to zero [4].

For the first layer of ACO-OFDM, the constellation symbols are mapped onto odd subcarriers, i.e., X_{2k+1} for $k = 0, 1, 2, \cdots, N/4 - 1$), in a frame and unused subcarriers are set to zero. After applying Hermitian symmetry, the frequency-domain symbol vector $\mathbf{X}^{(1)}$ is given by

$$\mathbf{X}^{(1)} = \left[0, X_1, 0, X_3, 0, \cdots, X_{N/2-1}, 0, X^*_{N/2-1}, \cdots, 0, X^*_1\right]. \tag{1}$$

In general, for the l-th layer ACO-OFDM ($l = 1, \cdots, L$ and $L < \log_2 N - 1$), define the index set of data bearing carriers (before Hermitian symmetry) as $\mathbb{K}^{(l)}_{\mathrm{ACO}} = \{2^{l-1}(2q+1), q = 0, 1, \cdots, \phi(l) - 1\}$ where

$$\phi(l) \triangleq \frac{N}{2^{l+1}}. \tag{2}$$

Therefore, for the l-th layer the constellation symbols are mapped onto X_k for $k \in \mathbb{K}^{(l)}_{\mathrm{ACO}}$, Hermitian symmetry is imposed and all other subcarriers are set to zero resulting in the frequency domain symbol

$$\mathbf{X}^{(l)} = [0, \cdots, 0, X_{2^{l-1}}, 0, \cdots, 0, X_{3\cdot 2^{l-1}}, 0, \cdots, 0, X^*_{2^{l-1}}, 0, \cdots, 0] \tag{3}$$

where there are $(2^l - 1)$ zeros in between two adjacent non-zero symbols.

Next, an N-point inverse fast Fourier transform (IFFT) is performed on $\mathbf{X}^{(l)}$ at l-th layer to obtain a bipolar time-domain signal vector $\mathbf{x}^{(l)}$, where the n-th element is defined as

$$x^{(l)}_n = \frac{1}{\sqrt{N}} \sum_{k=0}^{N-1} {X_k}^{(l)} \exp\left(j\frac{2\pi}{N}nk\right), \ 0 \le n \le N-1. \tag{4}$$

As shown in [9], $\mathbf{x}^{(l)}$ is a real-valued bipolar vector with a period of $4\phi(l) = \frac{N}{2^{l-1}}$, and has an anti-symmetry as

$$x^{(l)}_n = -x^{(l)}_{n+2\phi(l)}, \ 0 \le n \le 2\phi(l) - 1. \tag{5}$$

Therefore, the negative part of $\mathbf{x}^{(l)}$ can be directly clipped without losing any information leading to ACO-OFDM time-domain signal $\mathbf{x}^{(l)}_c$, which is given by [5]

$$x^{(l)}_{c,n} = \frac{1}{2}x^{(l)}_n + \frac{1}{2}\left|x^{(l)}_n\right| \tag{6}$$

where $|\cdot|$ denotes absolute value operation.

After L layers of ACO-OFDM, there remain $2\phi(L)$ subcarriers that are unused. In this work, AVO-OFDM [3] is employed to send data on these unused carriers. Note that L is a variable that must be designed to optimize the performance of ALACO-OFDM as shown in Sec. IV. Define $\mathbb{K}_{\text{AVO}} = \{q2^L, q = 1, \cdots, \phi(L) - 1\}$ as the index set of data bearing carriers (before Hermitian symmetry) for AVO-OFDM. Specifically, QAM symbols are mapped onto Y_k for $k \in \mathbb{K}_{\text{AVO}}$ with other subcarriers set to zero. After Hermitian symmetry, the frequency-domain symbol vector $\mathbf{Y}$ is given as

$$\mathbf{Y} = [0, \cdots, 0, Y_{2^L}, 0, \cdots, 0, Y_{2\cdot 2^L}, 0, \cdots, 0, Y^*_{2^L}, 0, \cdots, 0] \tag{7}$$

where there are $(2^L - 1)$ zeros in between two adjacent non-zero symbols. The time-domain signal y_n is obtained via the IFFT to give

$$y_n = \frac{1}{\sqrt{N}} \sum_{k=0}^{N-1} Y_k \exp\left(j\frac{2\pi}{N}nk\right),\ 0 \le n \le N-1. \tag{8}$$

Substituting (7) into (8) gives

$$y_n = \frac{1}{\sqrt{N}} \sum_{q=0}^{2\phi(L)-1} Y_{q2^L} \exp\left(j\frac{2\pi}{2\phi(L)}qn\right) \tag{9}$$

where $0 \le n \le N-1$. From (9), notice that $\mathbf{y}$ has a period of $2\phi(L)$, i.e.,

$$y_n = y_{n+2\phi(L)}. \tag{10}$$

To ensure non-negativity, define $y_{a,n}$ as

$$y_{a,n} = |y_n|,\ 0 \le n \le N-1. \tag{11}$$

Considering $\mathbf{y}$ has a period of $2\phi(L)$, only $2\phi(L)$ sign bits need to be transmitted to reconstruct the original AVO-OFDM signal. Let the vector of sign bits be denoted as $\mathbf{s}$, with components [3]

$$s_n = \begin{cases} 0, & y_n \le 0; \\ 1, & y_n > 0, \end{cases} \tag{12}$$

where $0 \le n \le 2\phi(L) - 1$. These sign bits are inserted uniformly over transmitting symbols mapped to symbol vector $\mathbf{X}^{(1)}$, which is transmitted by the first layer ACO-OFDM.

Adding together the L layer ACO-OFDM signals $\mathbf{x}_c^{(l)}$ and the AVO-OFDM signal $\mathbf{y}_a$, the discrete time-domain transmitted signal vector is denoted $\mathbf{z}$ with components

$$z_n = \sum_{l=1}^{L} x_{c,n}^{(l)} + y_{a,n},\ 0 \le n \le N-1. \tag{13}$$

Finally, after parallel-to-serial (P/S) conversion and the addition of a cyclic prefix (CP), $\mathbf{z}$ is fed into a digital-to-analog (D/A) converter before driving an LED.

B. Receiver

At the receiver, a photo-diode (PD) converts the received optical signal into an electrical current. The shot noise and thermal noise are modelled as additive white Gaussian noise (AWGN) [5], [9]. As this paper focuses on transceiver design, here we consider a flat channel with perfect equalization and synchronization are assumed and the channel gain from the LED to the PD is assumed to be unity [5], [6].

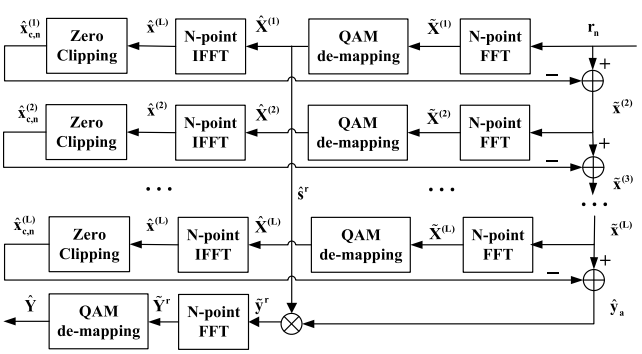

Fig. 2. Receiver design block diagram for ALACO-OFDM.

The receiver block diagram is depicted in Fig. 2. After S/P conversion, analog-to-digital (A/D) conversion and removal of the CP, the received signal r_n is

$$r_n = z_n + w_n,\ 0 \le n \le N-1 \tag{14}$$

where w_n is zero mean AWGN with variance σ_w^2.

It is well known that the clipping distortion of l-th ($1 \le l \le L$) layer ACO-OFDM falls on subcarriers of higher layers; i.e., the l-th layer ACO-OFDM must be demodulated before the $(l+1)$-th layer [9]. It can also be shown that the AVO-OFDM layer has components solely at frequencies indices in $\mathbb{K}_{\text{AVO}}$ and Hermitian symmetric components and thus does not interfere with any of the ACO-OFDM layers [12]. Thus, demodulation starts at the first ACO-OFDM layer and clipping noise is successively removed from lower layer signals.

For the demodulation of the first layer, $\mathbf{r}$ is fed into a fast Fourier transform (FFT) module to generate its DFT symbol vector, denoted as $\widetilde{\mathbf{X}}^{(1)}$ in Fig. 2 with elements

$$\widetilde{X}_k^{(1)} = \frac{1}{\sqrt{N}} \sum_{n=0}^{N-1} r_n \exp\left(-j\frac{2\pi}{N}nk\right),\ 0 \le k \le N-1. \tag{15}$$

This vector is then utilized to detect the modulated symbols at the first layer as

$$\widehat{X}_k^{(1)} = \arg \min_{X \in \Omega_X^{(1)}} \left\| X - 2\widetilde{X}_k^{(1)} \right\|^2,\ k = 1, 3, \cdots, N/2 - 1 \tag{16}$$

where $\Omega_X^{(1)}$ denotes the constellation set of symbols at the first layer and the scalar 2 is due to the zero clipping loss [9].

An ACO-OFDM time-domain signal local estimation $\widehat{x}_{c,n}^{(1)}$ can be generated using an IFFT and clipping, as shown in Fig. 2. The signal $\widehat{x}_{c,n}^{(1)}$ is subtracted from the received signal r_n leading to $\widetilde{x}_n^{(2)}$ that is employed to demodulate the symbols at the second layer.

Demodulation of the subsequent ACO-OFDM layers proceeds in a similar fashion where at layer l, QAM symbols are detected to the DFT symbol vector $\widetilde{\mathbf{X}}^{(l)}$ which arises as the FFT of $\widetilde{\mathbf{x}}^{(l)} = \widetilde{\mathbf{x}}^{(l-1)} - \widehat{\mathbf{x}}_c^{(l-1)}$, i.e., the impact of the detected

symbols in the previous layers is removed from subsequent layers.

After the L-th ACO-OFDM layer is detected, the clipping noise on the carriers in $\mathbb{K}_{\text{AVO}}$ can be removed by computing the local estimate of $\widehat{\mathbf{x}}_c^{(L)}$ and subtracting it from the remaining signal vector $\widetilde{\mathbf{x}}^{(L)}$. More compactly, an estimate of the AVO-OFDM signal $\widehat{\mathbf{y}}_a = \widetilde{\mathbf{x}}^{(L)} - \widehat{\mathbf{x}}_c^{(L)}$.

In order to be able to demodulate the data in the AVO-OFDM signal, the sign information must be extracted from the first layer of ACO-OFDM. Let $\widehat{s}_n$ denote the detected sign information of the AVO-OFDM signal that is transmitted in layer one. Furthermore, let $\widehat{s}_n^r \in \{-1, 1\}$ denote the sign of the $\widehat{y}_{a,n}$ which is extracted for the first $2\phi(L)$ symbols by

$$\widehat{s}_n^r = \begin{cases} 1, & \widehat{s}_n = 1; \\ -1, & \widehat{s}_n = 0, \end{cases} \tag{17}$$

where $n = 0, \cdots, 2\phi(L) - 1$. As noted in (10), the AVO-OFDM signal is periodic with period $2\phi(L)$ and thus, $\widehat{s}_n^r$ can be readily extended for all $n = 0, \cdots, N-1$.

The AVO-OFDM time-domain signal can be reconstructed as

$$\widehat{y}_n^r = \widehat{s}_n^r \widehat{y}_{a,n}, \ n = 0, 1, 2, \cdots, N-1. \tag{18}$$

After an N-point FFT module, the AVO-OFDM symbols can be detected using

$$\widehat{Y}_k = \arg \min_{Y \in \Omega_Y} \left\| Y - \widehat{Y}_k^r \right\|^2 \tag{19}$$

where Ω_Y denotes the constellation set of AVO-OFDM, $\widehat{Y}_k^r$ denotes the DFT of $\widehat{y}_n^r$ and $k \in \mathbb{K}_{\text{AVO}}$.

III. ALACO-OFDM Signal Analysis

In this section, the spectral efficiency and computational complexity of ALACO- are analyzed and compared to eU- [6], LACO- [9] and AAO-OFDM [3].

A. Spectral Efficiency

In this work, the spectral efficiency is defined as information rate per channel use. Hence, the spectral efficiency of DCO-OFDM with QAM constellation size M, Υ_{DCO}, can be written as

$$\Upsilon_{\text{DCO}} = \frac{1}{2} \log_2 M \text{ bits/channel use.} \tag{20}$$

The spectral efficiency of eU-OFDM with L streams, $\Upsilon_{\text{eU}}^{(L)}$, and of LACO-OFDM with L layers, $\Upsilon_{\text{LA}}^{(L)}$, are equal, and take the form [6], [9]

$$\Upsilon_{\text{LA}}^{(L)} = \frac{1}{2} \log_2 M - \frac{1}{2^{L+1}} \log_2 M \text{ bits/channel use,} \tag{21}$$

in which each stream/layer is assumed to use the same constellation size M.

The spectral efficiency of AAO-OFDM, Υ_{AAO}, can be calculated by [3]

$$\Upsilon_{\text{AAO}} = \frac{1}{4}(\log_2 M_1 + \log_2 M_2) - \frac{1}{2} \text{ bits/channel use,} \tag{22}$$

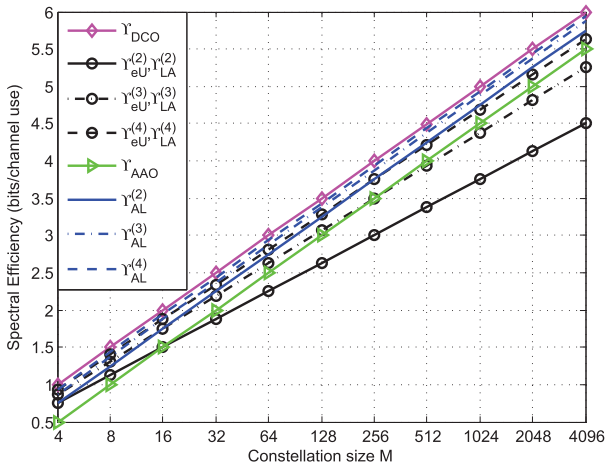

Fig. 3. The spectral efficiency comparison between ALACO-OFDM and its counterparts with different constellation sizes.

in which the constellation size M_1 and M_2 are assumed for AVO-OFDM and ACO-OFDM component parts, respectively. In the case of $M_1 = M_2 = M$

$$\Upsilon_{\text{AAO}} = \frac{1}{2} \log_2 M - \frac{1}{2} \text{ bits/channel use.} \tag{23}$$

For ALACO-OFDM, for the l-th ($1 \le l \le L$) layer ACO-OFDM, let M_l denote the size of the constellation sent on each ACO-OFDM layer. Note that there are $\phi(l) = \frac{N}{2^{l+1}}$ effective complex symbols before Hermitian symmetry for each ACO-OFDM layer l. For AVO-OFDM, the constellation size is denoted M_v and there are $\phi(L) - 1 = \frac{N}{2^{L+1}} - 1$ effective complex symbols before Hermitian symmetry. Notice also that $2\phi(L) = \frac{N}{2^L}$ sign bits of AVO-OFDM time-domain signals are inserted uniformly into transmitting symbols at the first layer.

Hence, the spectral efficiency of ALACO-OFDM with L layers, denoted by $\Upsilon_{\text{AL}}^{(L)}$, is

$$\begin{aligned} \Upsilon_{\text{AL}}^{(L)} &= \frac{1}{N} \left(\sum_{l=1}^{L} \frac{N}{2^{l+1}} \log_2 M_l + \left(\frac{N}{2^{L+1}} - 1 \right) \log_2 M_v - \frac{N}{2^L} \right) \\ &\approx \sum_{l=1}^{L} \frac{1}{2^{l+1}} \log_2 M_l + \frac{1}{2^{L+1}} \log_2 M_v - \frac{1}{2^L} \end{aligned} \tag{24}$$

where the approximation holds for large N.

If $M_l = M_v = M$, $\Upsilon_{\text{AL}}^{(L)}$ can be rewritten as

$$\Upsilon_{\text{AL}}^{(L)} = \frac{1}{2} \log_2 M - \frac{1}{2^L} \text{ bits/channel use.} \tag{25}$$

Notice that AAO-OFDM is a special case of ALACO-OFDM with $L = 1$ according to (23) and (25).

The spectral efficiency comparison between ALACO- and DCO-, eU-, LACO- and AAO-OFDM for large N is depicted with different constellation sizes in Fig. 3. It can be seen that Υ_{AAO}, $\Upsilon_{\text{AL}}^{(2)}$, $\Upsilon_{\text{AL}}^{(3)}$, $\Upsilon_{\text{AL}}^{(4)}$ and Υ_{DCO} are parallel, which indicates a constant gap between them. Additionally, notice that ALACO-OFDM is closest to the spectral efficiency of DCO-OFDM. The difference in spectral efficiency between ALACO- and DCO-OFDM decreases with increasing L as $1/2^L$. For example, for $L = 2$ ALACO-OFDM 0.25

bits/channel use less than DCO-OFDM, while at $L = 4$ the difference is only 0.0625 bits/channel use. For eU-OFDM and LACO-OFDM, the larger the constellation size, the larger the spectral-efficiency gap compared to DCO-OFDM. When $M > 256$, ALACO-OFDM with $L = 2$ achieves larger spectral efficiency than eU-OFDM and LACO-OFDM with $L = 4$. For the same layer number L, the spectral efficiency of ALACO-OFDM is

$$\frac{\log_2 M - 2}{2^{L+1}} \quad \text{bits/channel use}$$

larger than eU-OFDM and LACO-OFDM.

B. Computational Complexity

For an N-point (N a power of 2) IFFT or FFT module using the Cooley-Tukey decomposition, $M(N)$ real-valued multiplication operations (RMOs) and $A(N)$ real-valued addition operations (RAOs) are required where [13]

$$M(N) = 2N\log_2(N) - 4N + 4 \tag{26}$$

and

$$A(N) = 3N\log_2(N) - 2N + 2. \tag{27}$$

In the subsequent analysis, we assume that operations such as zero clipping, taking the sign bits, and absolute value operation do not require any arithmetic operations as they can be efficiently implemented via switching logic. In addition, the complexity of detecting QAM symbols on carriers is the same for all schemes thus is not included in this analysis.

Though the N-point IFFT and FFT in Fig. 1 and 2 are useful in depicting the basic idea of ALACO-OFDM transceiver design, more efficient approaches have been documented in the literature. For LACO- and ALACO-OFDM, to reduce the complexity, a $4\phi(l)$-point IFFT can be employed and repeated 2^{l-1} times for l-th ACO-OFDM layer as shown in [9]. A $2\phi(L)$-point IFFT can similarly to used and repeated 2^L times for AVO-OFDM layer due to the periodic property of $\mathbf{y}$. At the receiver, averaging is required in the time domain over 2^{l-1} periods for l-th ACO-OFDM layer and over 2^L periods for AVO-OFDM layer to enhance the performance. These two approaches to the implementation layered ACO-OFDM have been included in the following analysis.

1) Transmitter: For DCO-OFDM, an N-point IFFT module is required at transmitter and it requires $M^{(t)}_{\text{DCO}}(N) = M(N)$ RMOs and $A^{(t)}_{\text{DCO}}(N) = A(N)$ RAOs.

For ALACO-OFDM, the required RMOs and RAOs of ALACO-OFDM can be written as

$$\begin{aligned} &M^{(t)}_{\text{AL}}(L,N) \\ &= \sum_{l=1}^{L} M\left(\frac{N}{2^{l-1}}\right) + M\left(\frac{N}{2^L}\right) \\ &= \left(1 - \frac{1}{2^{L+1}}\right) 4N\log_2(N) - \left(12 - \frac{L+4}{2^{L-1}}\right) N + 4L + 4 \end{aligned} \tag{28}$$

and

$$\begin{aligned} &A^{(t)}_{\text{AL}}(L,N) \\ &= \sum_{l=1}^{L} A\left(\frac{N}{2^{l-1}}\right) + A\left(\frac{N}{2^L}\right) + LN \\ &= \left(1 - \frac{1}{2^{L+1}}\right) 6N\log_2(N) - \left(11 - L - \frac{3L+8}{2^L}\right) N \\ &\quad + 2L + 2. \end{aligned} \tag{29}$$

Similarly, for LACO-OFDM with N subcarriers and L layers, the required RMOs and RAOs are given by

$$\begin{aligned} &M^{(t)}_{\text{LA}}(L,N) \\ &= \sum_{l=1}^{L} M\left(\frac{N}{2^{l-1}}\right) \\ &= \left(1 - \frac{1}{2^L}\right) 4N\log_2(N) - \left(12 - \frac{2L+6}{2^{L-1}}\right) N + 4L \end{aligned} \tag{30}$$

and

$$\begin{aligned} &A^{(t)}_{\text{LA}}(L,N) \\ &= \sum_{l=1}^{L} A\left(\frac{N}{2^{l-1}}\right) + (L-1)N \\ &= \left(1 - \frac{1}{2^L}\right) 6N\log_2(N) - \left(11 - L - \frac{3L+5}{2^{L-1}}\right) N + 2L. \end{aligned} \tag{31}$$

For eU-OFDM with N subcarriers and L streams, there are 2^L OFDM frames included in one super frame. Hence, RMOs and RAOs averaged over a super frame are [14]

$$M^{(t)}_{\text{eU}}(L,N) = \left(1 - \frac{1}{2^L}\right)(2N\log_2(N) - 4N + 4) \tag{32}$$

and

$$\begin{aligned} &A^{(t)}_{\text{eU}}(L,N) \\ &\quad = \left(1 - \frac{1}{2^L}\right)(3N\log_2(N) - 2N + 2) + (L-1)N \end{aligned} \tag{33}$$

2) Receiver: For DCO-OFDM, an N-point FFT module is required at receiver and requires $M^{(r)}_{\text{DCO}}(N) = M(N)$ RMOs and $A^{(r)}_{\text{DCO}}(N) = A(N)$ RAOs.

For ALACO-OFDM, to detect the l-th layer of the ACO-OFDM signal ($1 \le l \le L$), an $4\phi(l)$-point FFT is required followed by an $4\phi(l)$-point IFFT for signal reconstruction. For AVO-OFDM layer, $2\phi(L)$-point FFT is required only for demodulation. Hence ALACO-OFDM requires $M^{(r)}_{\text{AL}}(L,N)$ RMOs as

$$\begin{aligned} &M^{(r)}_{\text{AL}}(L,N) \\ &= 2\sum_{l=1}^{L} M\left(\frac{N}{2^{l-1}}\right) + M\left(\frac{N}{2^L}\right) \\ &= \left(1 - \frac{3}{2^{L+2}}\right) 8N\log_2(N) - \left(24 - \frac{3L+10}{2^{L-1}}\right) N + 8L + 4 \end{aligned} \tag{34}$$

and RAOs as

$$A^{(r)}_{\text{AL}}(L,N)$$

$$= 2\sum_{l=1}^{L} A\left(\frac{N}{2^{l-1}}\right) + A\left(\frac{N}{2^{L}}\right) + \underbrace{\sum_{l=1}^{L}\left(2^{l-1}-1\right)\frac{N}{2^{l-1}} + \left(2^{L}-1\right)\frac{N}{2^{L}}}_{\text{Averaging for } L \text{ ACO layers and AVO}} + \underbrace{LN}_{\text{Removing low layers}}$$
$$= \left(1-\frac{3}{2^{L+2}}\right)12N\log_2(N) - \left(21-2L-\frac{9L+19}{2^{L}}\right)N + 4L + 2. \quad (35)$$

The conventional LACO-OFDM receiver [9] removes interference from lower layers in the frequency domain. In contrast, the receiver in Fig. 2 removes interference between layers at the receiver directly in the time domain. This approach requires fewer N-point FFTs than the receiver in [9] and is thus less complex. For the sake of fair comparison, the receiver for LACO-OFDM is computed when the interference is removed in the time domain (as shown for the first L layers in Fig. 2). The number of RMOs and RAOs for LACO-OFDM when interference is removed in time domain are

$$M_{\text{LA}}^{(r)}(L,N) = 2\sum_{l=1}^{L-1} M\left(\frac{N}{2^{l-1}}\right) + M\left(\frac{N}{2^{L-1}}\right) = \left(1-\frac{3}{2^{L+1}}\right)8N\log_2(N) - \left(24-\frac{6L+14}{2^{L-1}}\right)N + 8L - 4 \quad (36)$$

and

$$A_{\text{LA}}^{(r)}(L,N) = 2\sum_{l=1}^{L-1} A\left(\frac{N}{2^{l-1}}\right) + A\left(\frac{N}{2^{L-1}}\right) + \underbrace{\sum_{l=1}^{L}\left(2^{l-1}-1\right)\frac{N}{2^{l-1}}}_{\text{Averaging for } L \text{ ACO layers}} + \underbrace{(L-1)N}_{\text{Removing low layers}}$$
$$= \left(1-\frac{3}{2^{L+1}}\right)12N\log_2(N) - \left(23-2L-\frac{9L+10}{2^{L-1}}\right)N + 4L - 2. \quad (37)$$

For eU-OFDM with N subcarriers and L streams, the number of RMOs and RAOs on average over a super frame are [14]

$$M_{\text{eU}}^{(r)}(L,N) = \left(1-\frac{3}{2^{L+1}}\right)(4N\log_2(N) - 8N + 8) \quad (38)$$

and

$$A_{\text{eU}}^{(r)}(L,N) = \left(1-\frac{3}{2^{L+1}}\right)6N\log_2(N) - \left(6-2L-\frac{7}{2^{L}}\right)N + 4 - \frac{6}{2^{L}}. \quad (39)$$

Fig. 4 presents a comparison of the RMOs and RAOs for ALACO-, LACO- and eU-OFDM. Although for the same L, ALACO-OFDM requires slightly more RMOs and RAOs than LACO-OFDM, given the same *spectral efficiency* LACO-OFDM requires more layers and is more complex as compared to ALACO-OFDM. For example, ALACO-OFDM with $L = 2$ and $M = 256$ and LACO-OFDM with $L = 4$ and $M = 256$ achieve the same spectral efficiency of 3.75 bits/channel use. From Fig. 4, at transmitter, LACO-OFDM with $L = 4$ requires about 5% more RMOs and 7% more RAOs than ALACO-OFDM with $L = 2$. At receiver, LACO-OFDM requires about 9% more RMOs and 11% more RAOs than ALACO-OFDM when operating at the same spectral efficiency.

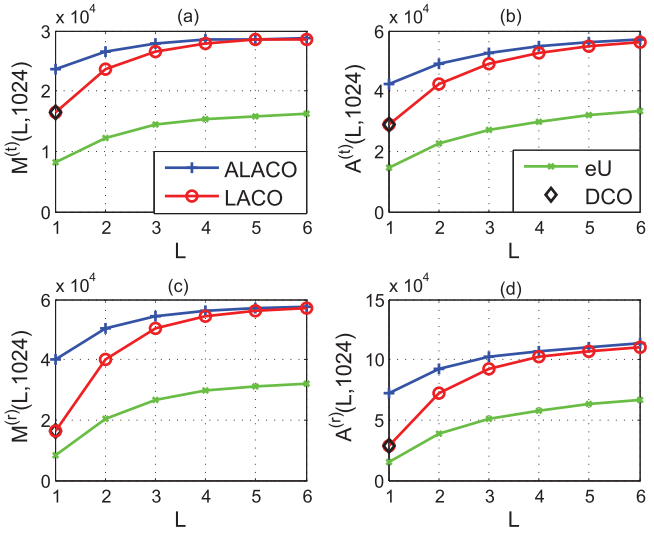

Fig. 4. Computational complexity comparison between ALACO-OFDM and its counterparts for different L ($N = 1024$ in all cases).

IV. Design of ALACO-OFDM Systems

Given that signals from different layers in ALACO-OFDM are combined to make the emitted signal, an open question is the allocation of optical power amongst the layers to ensure optimal performance. In this section, two optical power allocation schemes over the layers of ALACO-OFDM are discussed to optimize uncoded transmission performance and achievable information rates, respectively.

A. Signal Distributions, Optical and Electrical Power

Using the central limit theorem (CLT), the probability density function (PDF) of ACO-OFDM signal in the l-th layer is given by [5], [15]–[18]

$$f_l(w) = \frac{1}{\sqrt{2\pi}\sigma_l}\exp\left(\frac{-\xi^2}{2\sigma_l^2}\right)u(\xi) + \frac{1}{2}\delta(\xi) \quad (40)$$

where σ_l is the standard deviation of the ACO-OFDM signal in the l-th layer before clipping, (see $\mathbf{x}^{(l)}$ in Fig. 1), $u(\xi)$ is a unit step function and $\delta(\xi)$ is a unit impulse funtion. The average optical and electrical power of ACO-OFDM signal in the l-th layer can be calculated as [16], [18]

$$P_{o,l} = \frac{\sigma_l}{\sqrt{2\pi}} \quad \text{and} \quad P_{e,l} = \frac{\sigma_l^2}{2}. \quad (41)$$

For AVO-OFDM, the PDF of $y_{\mathrm{a},n}$ is a truncated Gaussian [3]

$$f_v(\xi) = \frac{2}{\sqrt{2\pi}\sigma_v}\exp\left(\frac{-\xi^2}{2\sigma_v^2}\right)u(\xi) \tag{42}$$

where σ_v is the standard deviation of AVO-OFDM signal before absolute value operation (see **y** in Fig. 1). Additionally, the average optical and electrical power of AVO-OFDM signal are [3]

$$P_{o,v} = \frac{2\sigma_v}{\sqrt{2\pi}} \quad \text{and} \quad P_{e,v} = \sigma_v^2. \tag{43}$$

Thus, the average optical power of ALACO-OFDM signal z_n in Fig. 1 is can be calculated by

$$P_{o,\mathrm{AL}} = \sum_{l=1}^{L} E\{x_{c,n}^{(l)}\} + E\{y_{a,n}\} = \frac{1}{\sqrt{2\pi}}\left(\sum_{l=1}^{L}\sigma_l + 2\sigma_v\right) \tag{44}$$

where $\mathrm{E}\{\cdot\}$ denotes the expectation operator.

After clipping, the transmitted signal for each layer in frequency domain can be decomposed into two orthogonal components following (6), as

$$X_{c,k}^{(l)} = \frac{1}{2}X_k^{(l)} + \frac{1}{2}X_{a,k}^{(l)} \tag{45}$$

where $\frac{1}{2}X_k^{(l)}$, $k \in \mathbb{K}_{\mathrm{ACO}}^{(l)}$ is the useful transmitted signal and $\frac{1}{2}X_{a,k}^{(l)}$ is clipping distortion.

After some straightforward manipulation, the average electrical power of data symbols falling onto each subcarrier in the l-th layer ACO-OFDM is given by (ignoring Hermitian symmetric components)

$$E\left\{\left|\frac{1}{2}X_k^{(l)}\right|^2\right\} = \begin{cases} 2^{l-2}\sigma_l^2, & k \in \mathbb{K}_{\mathrm{ACO}}^{(l)}, \\ 0, & \text{otherwise.} \end{cases} \tag{46}$$

Similarly, assuming that the sign information is recovered correctly, the average electrical power of data symbol in k-th subcarrier in AVO-OFDM is given by

$$E\{|Y_k|^2\} = \begin{cases} 2^L\sigma_v^2, & k \in \mathbb{K}_{\mathrm{AVO}}, \\ 0, & \text{otherwise.} \end{cases} \tag{47}$$

B. Optical Power Allocation - Uncoded Transmission

Consider an ALACO-OFDM system which operates under a fixed average optical power constraint, $P_{o,\mathrm{AL}}$. Such systems arise in VLC links with dimming constraints. Assume that the clipping distortion from lower layers is completely removed from higher layers which is reasonable at high SNRs. Additionally, assume a flat channel with AWGN noise in each subcarrier with variance σ_w^2. Let SNR_k denote the electrical SNR of the k-th subcarrier from (46) and (47) which governs the uncoded BER performance.

Here we consider the optimal allocation of optical power to each ALACO-OFDM layer subject to an average optical power constraint with the objective of optimizing the uncoded BER. In particular, the optimal power allocation is the one which selects σ_l and σ_v over ALACO-OFDM layers which maximizes the minimum SNR over all data-bearing subcarriers while satisfying the average optical power constraint (44). More precisely,

$$\mathbf{P1}: \max_{\sigma_l,\,\sigma_v} \quad \min_k \mathrm{SNR}_k \tag{48a}$$

$$\text{s.t.} \quad \mathrm{SNR}_k = \begin{cases} \frac{2^{l-2}\sigma_l^2}{\sigma_w^2}, k \in \mathbb{K}_{\mathrm{ACO}}^{(l)},\ 1 \le l \le L, \\ \frac{2^L\sigma_v^2}{\sigma_w^2}, k \in \mathbb{K}_{\mathrm{AVO}}, \end{cases} \tag{48b}$$

$$\sum_{l=1}^{L}\sigma_l + 2\sigma_v = \sqrt{2\pi}P_{o,\mathrm{AL}}, \tag{48c}$$

$$\sigma_l \ge 0,\ 1 \le l \le L, \tag{48d}$$

$$\sigma_v \ge 0. \tag{48e}$$

Since $\mathrm{SNR}_k \ge 0$, taking the square root of SNR_k linearizes the optimization problem as

$$\mathbf{P2}: \min_{\sigma_l,t} \quad -t \tag{49a}$$

$$\text{s.t.} \quad 2^{\frac{l-2}{2}}\frac{\sigma_l}{\sigma_w} \ge t, k \in \mathbb{K}_{\mathrm{ACO}}^{(l)},\ 1 \le l \le L, \tag{49b}$$

$$2^{\frac{L}{2}}\frac{\sigma_v}{\sigma_w} \ge t, k \in \mathbb{K}_{\mathrm{AVO}}, \tag{49c}$$

$$(48c) - (48e). \tag{49d}$$

The objective function and constraints of **P2** are affine, which can be solved easily through Karush-Kuhn-Tucker (KKT) method. The solutions are given as

$$\sigma_l^\star = \frac{2^{-\frac{l-2}{2}}\sqrt{\pi}P_{o,\mathrm{AL}}}{A},\ 1 \le l \le L, \tag{50a}$$

$$\sigma_v^\star = \frac{2^{-\frac{L}{2}}\sqrt{\pi}P_{o,\mathrm{AL}}}{A} \tag{50b}$$

where for readability, $A \triangleq 2 + \sqrt{2} - 2^{-(L-2)/2}$. Substituting (50) into (41) and (43), we can obtain the optimal optical power $P_{o,l}^\star$ and $P_{o,v}^\star$.

Notice that using the optimum power allocation $\sigma_l^\star$ and $\sigma_v^\star$ yields the same SNR_k for all data bearing subcarriers regardless of their layer, that is

$$\mathrm{SNR}_k = \frac{\pi}{A^2}\frac{P_{o,\mathrm{AL}}^2}{\sigma_w^2}. \tag{51}$$

This result corresponds to the empirically chosen power allocations used in previous work [9], [18]. Section V presents numerical investigation of (50) over different choices of power allocation.

Define power allocation factor α as the ratio between optical power of adjacent ACO-OFDM layers, i.e.,

$$\alpha \triangleq \frac{P_{o,l}}{P_{o,l+1}},\ 1 \le l \le L-1. \tag{52}$$

Notice that using the optimum power allocation $\sigma_l^\star$ and $\sigma_v^\star$ in (50), $\alpha = \sqrt{2}$ and $P_{o,v} = P_{o,L}$. This result matches previous empirically derived power allocations in [9], [18]–[21] and [3] for LACO- and AAO-OFDM respectively. In a related context, [16] also conclude that LACO-OFDM achieves optimal power allocation with $\alpha = \sqrt{2}$ under an electrical power constraint.

C. Optical Power Allocation - Information Rate

Here, the optical power allocation amongst ALACO-OFDM layers is done to maximize the overall achievable information rate under an average optical power constraint.

1) Achievable Information Rate of ALACO-OFDM: For the l-th layer ACO-OFDM, an optical power constraint leads to an electrical power constraint according to (41) and (46), hence Shannon capacity formula in [22] can be employed [15]. In addition, there are $\frac{N}{2^{l+1}}$ out of N subcarriers bearing data symbols before Hermitian symmetry. The achievable information rate for l-th ACO-OFDM layer was first derived in [23] as

$$C_l = \frac{1}{2^{l+1}} \log\left(1 + \frac{2^{l-2}\sigma_l^2}{\sigma_w^2}\right) \text{ bits/channel use.} \quad (53)$$

For the AVO-OFDM layer, consider the following theorem.

Theorem 1: Consider an absolute-value Gaussian random variable channel, i.e., $z = y + w$, where $y = |x|$, x is real and Gaussian distributed with zero mean and variance of σ_x^2, and w is AWGN with variance of σ_w^2. The achievable information rate of this absolute-value Gaussian channel is

$$C_v = \frac{1}{2}\log\left(1 + \frac{\sigma_x^2}{\sigma_w^2}\right) - (1 - D) \quad (54)$$

where D is a monotonically decreasing function of $\gamma = \sigma_x/\sigma_w$, $0 < D \leq 1$ and $D \to 0$ as $\gamma \to \infty$.

Proof: See Appendix A. ∎

For AVO-OFDM, $\phi(L)$ out of N complex channels bear data (before Hermitian symmetry). Hence, according to Thm. 1, the achievable information rate for AVO-OFDM is

$$C_{\text{avo}} = \frac{1}{2^{L+1}}\log\left(1 + \frac{2^L\sigma_v^2}{\sigma_w^2}\right) - \frac{1}{2^L}(1 - D) \text{ bits/channel use.} \quad (55)$$

The achievable information rate of ALACO-OFDM can be bounded by the sum of achievable information rates of L layers of ACO-OFDM, the AVO-OFDM layer and subtracting the sign bits carried in the first layer to give

$$\begin{aligned} C_{\text{AL}}^{(L)} &= \sum_{l=1}^{L} C_l + C_{\text{avo}} - \frac{1}{2^L} \\ &= \sum_{l=1}^{L} \frac{1}{2^{l+1}}\log\left(1 + \frac{2^{l-2}\sigma_l^2}{\sigma_w^2}\right) \\ &\quad + \frac{1}{2^{L+1}}\log\left(1 + \frac{2^L\sigma_v^2}{\sigma_w^2}\right) - \frac{1}{2^{L-1}} + \frac{D}{2^L}, \ \ C_1 \geq \frac{1}{2^L}. \end{aligned} \quad (56)$$

2) Optimization Problem: Most VLC channels operate in the high SNR regime [25], [26]. At high SNRs, $C_{\text{AL}}^{(L)}$ can be approximated as

$$\tilde{C}_{\text{AL}}^{(L)} \approx \sum_{l=1}^{L} \frac{1}{2^l}\log\left(\frac{2^{\frac{l-2}{2}}\sigma_l}{\sigma_w}\right) + \frac{1}{2^L}\log\left(\frac{2^{\frac{L}{2}}\sigma_v}{\sigma_w}\right) - \frac{1}{2^{L-1}} \quad (57)$$

since at high SNR $D \to 0$ according to Thm. 1.

Consider an optimal power allocation over the ALACO-OFDM layers to maximize the capacity at high SNR, as approximated by $\tilde{C}_{\text{AL}}^{(L)}$, given formally as

$$\mathbf{P3}: \max_{\sigma_l, \sigma_v} \tilde{C}_{\text{AL}}^{(L)} \quad (58a)$$

$$\text{s.t.} \quad (48c) - (48e). \quad (58b)$$

The objective is the sum of concave functions and is thus also concave with the constraints are affine. Hence, an optimal solution can be obtained by solving the KKT conditions as

$$\tilde{\sigma}_l = \frac{\sqrt{2\pi}P_{o,\text{AL}}}{2^l}, \ 1 \leq l \leq L, \quad (59a)$$

$$\tilde{\sigma}_v = \frac{\sqrt{2\pi}P_{o,\text{AL}}}{2^{L+1}}. \quad (59b)$$

Notice that the optical power allocation factor, defined in (52), for the capacity optimal power allocation is $\alpha = 2$ which is similar to the result reported in [23], [24]. Substituting (59) into (41) and (43), the optimal optical power $\tilde{P}_{o,l}$ and $\tilde{P}_{o,v}$ can also be obtained.

Substituting (59) into (56), a lower bound on the achievable information rate of ALACO-OFDM is

$$\begin{aligned} \hat{C}_{\text{AL}}^{(L)} &= \sum_{l=1}^{L} \frac{1}{2^{l+1}}\log\left(1 + \frac{\pi P_{o,\text{AL}}^2}{2^{l+1}\sigma_w^2}\right) - \frac{1}{2^{L-1}} \\ &\quad + \frac{1}{2^{L+1}}\log\left(1 + \frac{\pi P_{o,\text{AL}}^2}{2^{L+1}\sigma_w^2}\right) + \frac{D}{2^L} \text{ bits/channel use.} \end{aligned} \quad (60)$$

Similarly, the achievable information rate of LACO-OFDM with $\alpha = 2$ can be bounded by the sum of the rates of L layers of ACO-OFDM as

$$C_{\text{LA}}^{(L)} = \sum_{l=1}^{L} \frac{1}{2^{l+1}}\log\left(1 + \frac{\pi P_{o,\text{AL}}^2}{2^{l-1}\left(2 - 2^{-(L-1)}\right)^2\sigma_w^2}\right). \quad (61)$$

Note that in the limiting case for large L and at high SNRs, the capacities of LACO- and ALACO-OFDM are equal according to (60) and (61) and approach

$$C_{\alpha=2} = \frac{1}{2}\log\left(\frac{\pi P_{o,\text{AL}}^2}{8\sigma_w^2}\right) \text{ bits/channel use.} \quad (62)$$

This asymptotic result has also been presented in [23].

D. Comparison Between Power Allocation Schemes

For the sake of comparison with previous work, define the optical SNR (OSNR) as in [23], [24], [26], [27]

$$\text{OSNR(dB)} = 10\log_{10}\left(\frac{P_{o,\text{AL}}}{\sigma_w}\right). \quad (63)$$

From Sec. IV-B, ALACO-OFDM achieves optimal uncoded transmission performance with $\alpha = \sqrt{2}$ while the high SNR information optimal allocations has $\alpha = 2$ according to Sec. IV-C.

Substituting (50) into (56), the achievable information rate of ALACO-OFDM with $\alpha = \sqrt{2}$ is

$$C_{\text{AL}}^{(L)} = \frac{1}{2}\log\left(1 + \frac{\pi}{A^2}\frac{P_{o,\text{AL}}^2}{\sigma_w^2}\right)$$

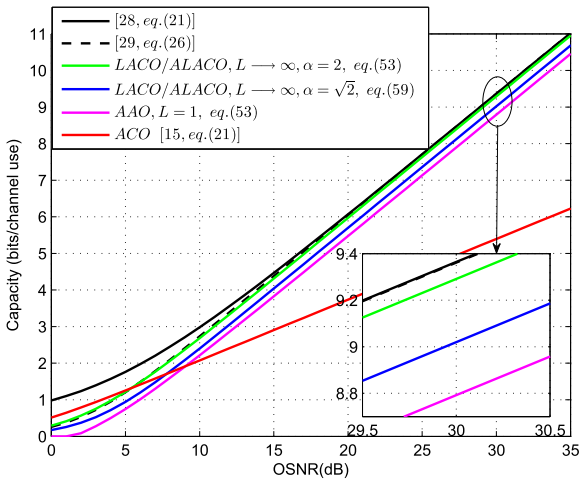

Fig. 5. Achievable information rate comparison among ACO-, LACO-, ALACO- and AAO-OFDM for different OSNR.

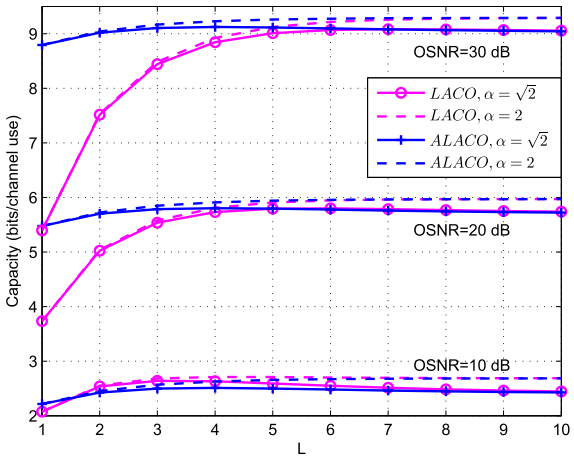

Fig. 6. Achievable information rate comparison between ALACO- and LACO-OFDM for different OSNRs and L layers (Note: L denotes the number of ACO-OFDM layers used).

$$-\frac{1}{2^{L-1}}+\frac{D}{2^{L}} \text{ bits/channel use.} \tag{64}$$

Similarly, for LACO-OFDM with $\alpha=\sqrt{2}$,

$$C_{\text{LA}}^{(L)}=\left(\frac{1}{2}-\frac{1}{2^{L+1}}\right)\log\left(1+\frac{\pi}{B^2}\frac{P_{o,\text{LA}}^2}{\sigma_w^2}\right) \text{ bits/channel use} \tag{65}$$

where $B\triangleq 2+\sqrt{2}-2^{-(L-2)/2}-2^{-(L-1)/2}$.

In the limit of large L and OSNR, the performance of LACO- and ALACO-OFDM with $\alpha=\sqrt{2}$ are identical and are given as

$$C_{\alpha=\sqrt{2}}=\frac{1}{2}\log\left(1+\frac{\pi}{6+4\sqrt{2}}\frac{P_{o,\text{AL}}^2}{\sigma_w^2}\right) \text{ bits/channel use.} \tag{66}$$

Subtracting (66) from (62), the asymptotic gap in information rate between the both optical power allocation schemes, i.e., $\alpha=2$ and $\alpha=\sqrt{2}$, is

$$\triangle C\approx\frac{1}{2}\log\left(\frac{6+4\sqrt{2}}{8}\right)=0.27 \text{ bits/channel use.} \tag{67}$$

Figure 5 presents a comparison of the information rate among ACO-, LACO-, ALACO-, and AAO-OFDM for different OSNR and power allocation schemes. Note that AAO-OFDM is a special case of ALACO-OFDM with $L=1$, i.e., the information rate of AAO-OFDM is given by $C_{\text{AL}}^{(1)}$. An upper bound on capacity of IM/DD optical channel based on sphere packing [28] and a lower bound based on entropy power inequality (EPI) and exponentially distributed input [29] are added as the benchmarks. It can be seen ALACO- and LACO-OFDM with $\alpha=2$ achieves higher information rate than that with $\alpha=\sqrt{2}$. And the gap is about 0.27 bits/channel use at OSNR$=30$ dB that agrees well with (67). Although ALACO- and LACO-OFDM with $\alpha=2$ can achieve higher capacity at high OSNR, its uncoded BER performance is worse than that with $\alpha=\sqrt{2}$, which is shown in Fig. 7.

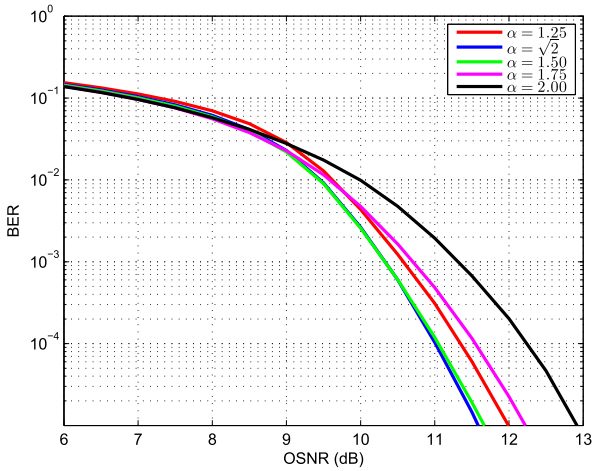

Fig. 7. Overall uncoded BER performance of ALACO-OFDM with different optical power allocation factor α with $L=3$ and $M=16$ used.

Figure 6 presents the achievable information rate comparison between ALACO- and LACO-OFDM for different number of layers and OSNRs. It is evident that ALACO-OFDM achieves higher rate than LACO-OFDM with a smaller number of layers at high OSNR.

Specifically, for $\alpha=\sqrt{2}$, when OSNR $=20$ dB, ALACO-OFDM with $L=3$ achieves 5.8 bits/channel use, which is higher than the highest achievable information rate of LACO-OFDM with $L=6$. When OSNR $=30$ dB, ALACO-OFDM achieves the highest achievable information rate with $L=4$, which is larger than the highest achievable information rate of LACO-OFDM with $L=7$. However, when OSNR $=10$ dB, LACO-OFDM achieve highest achievable information rate with $L=3$ and is slightly higher than ALCO-OFDM. This is because of the increased overhead in transmitting the sign information in the first layer. Similar conclusions hold for $\alpha=2$ where ALACO- can still achieve higher rate than LACO-OFDM with fewer number of layers.

Notice that the difference between the achievable information rates of ALACO- and LACO-OFDM becomes smaller as number of layers increases. This is because ALACO-OFDM is defined to use all the available subcarriers, and the number

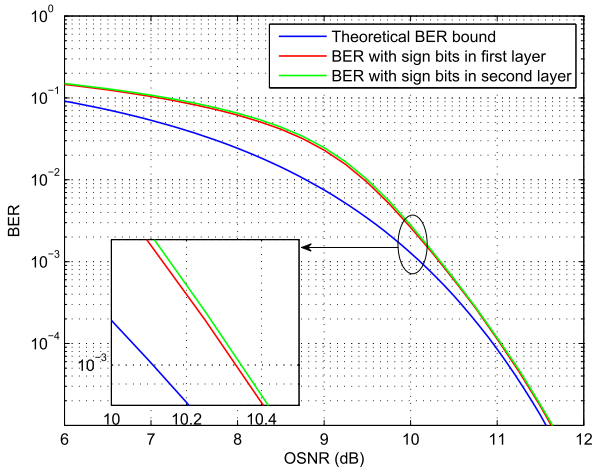

Fig. 8. Theoretical and simulated overall BER with sign bits in first layer and in second layer with $L = 3$ and $M = 16$ used.

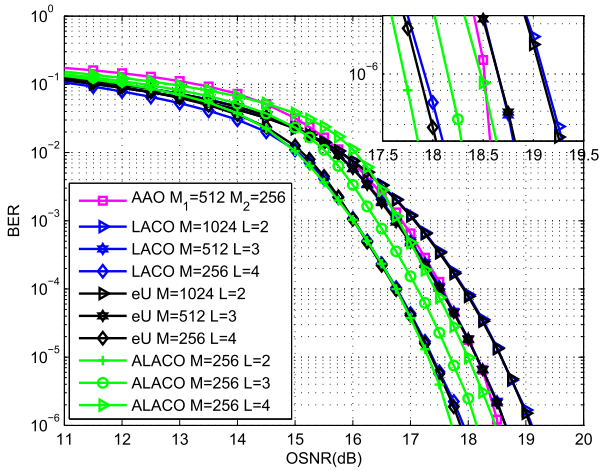

Fig. 9. Uncoded BER performance comparison between ALACO-OFDM and its counterparts with the same or close spectral efficiency (Set $\Upsilon_{\text{AAO}} = \Upsilon_{\text{eU}}^{(2)} = \Upsilon_{\text{LA}}^{(2)} = \Upsilon_{\text{AL}}^{(2)} = \Upsilon_{\text{eU}}^{(4)} = \Upsilon_{\text{LA}}^{(4)} = 3.75$ bits/channel use, $\Upsilon_{\text{eU}}^{(3)} = \Upsilon_{\text{LA}}^{(3)} = \Upsilon_{\text{AL}}^{(4)} = 3.9375$ bits/channel use, and $\Upsilon_{\text{AL}}^{(3)} = 3.875$ bits/channel use).

of unused subcarriers in LACO-OFDM approaches zero as L becomes large.

V. Numerical Results

A. BER Performance

In this section, uncoded BER performance of ALACO-OFDM is analyzed and compared to its counterparts in terms of OSNR. A flat channel with AWGN is assumed and the channel gain from an LED to a PD is assumed to be unity [5], [6]. Considering a flat channel and mitigating the effect of error propagation in layered OFDM schemes, the sign bits of the AVO-OFDM layer are uniformly inserted into the bits modulated in the first ACO-OFDM layer. The total number of subcarriers is set to $N = 1024$ and M-QAM constellations with gray labeling are utilized.

The overall BER performance of ALACO-OFDM with $M = 16$ and $L = 3$ for different α are shown in Fig. 7. It can be seen ALACO-OFDM with power allocation factor $\alpha = \sqrt{2}$ achieves optimal BER performance in high OSNR regime. ALACO with $\alpha = \sqrt{2}$ achieves about 1.3 dB gains compared to that with $\alpha = 2$ at BER$= 10^{-5}$. Hence, the optical power allocation factor is set to $\alpha = \sqrt{2}$ for ALACO-, LACO- and eU-OFDM in Fig. 8, Fig. 9, Fig. 10 and Fig. 11.

Using the formula for calculating the BER of QAM [18], [30], a theoretical bound on the BER of ALACO-OFDM can be given by

$$\text{BER}_{\text{AL}} = \frac{\sum_{l=1}^{L} \text{BER}_{\text{ACO}}^{(l)} 2^{-l} \log_2 M_l + \text{BER}_{\text{AVO}} 2^{-L} \log_2 M_v}{\sum_{l=1}^{L} 2^{-l} \log_2 M_l + 2^{-L} \log_2 M_v} \tag{68}$$

where $\text{BER}_{\text{ACO}}^{(l)}$ is BER of l-th layer ACO-OFDM, given by

$$\text{BER}_{\text{ACO}}^{(l)} \approx \frac{4(\sqrt{M_1}-1)}{\sqrt{M_1}\log_2 M_1} Q\left(\sqrt{\frac{3}{M_1-1}\frac{2^{l-2}\sigma_l^2}{\sigma_w^2}}\right), \tag{69}$$

and BER_{AVO} is BER of AVO-OFDM, given by

$$\text{BER}_{\text{AVO}} \approx \frac{4(\sqrt{M_v}-1)}{\sqrt{M_v}\log_2 M_v} Q\left(\sqrt{\frac{3}{M_v-1}\frac{2^{L}\sigma_v^2}{\sigma_w^2}}\right). \tag{70}$$

"$\approx$" is used in (69) and (70) since we assume the interference from lower layers is removed completely.

Theoretical and simulated overall BER with sign bits in first layer and in second layer are shown in Fig. 8, in which $L = 3$, $\alpha = \sqrt{2}$ and $M = 16$ are used. It can be seen ALACO-OFDM with sign bits carried in first layer slightly outperforms that with sign bits in second layer in low OSNR regime, while both perform nearly the same in high OSNR regime. This is because sign bits carried in second layer are distorted by AWGN and estimation error accumulated from the first layer, which slightly worsens the overall BER performance. As OSNR increases, the estimation error in first layer becomes negligible [12]. The theoretical bound on BER is also shown in Fig. 8, which is close to the simulated overall BER in high OSNR regime.

The BER performance of ALACO- is compared to eU-, LACO- and AAO-OFDM is shown in Fig. 9 with the same spectral efficiency and a finite number of layers. Notice that AAO-OFDM is the special case of the ALACO-OFDM with $L = 1$ and the both share the same performance. For ALACO-OFDM, $M = 256$ with $L = 2$, 3 or 4 is employed, of which has spectral efficiency is $\Upsilon_{\text{AL}}^{(L)} = 3.75$, 3.875 or 3.9375 bits/channel use according to (25). For eU- and LACO-OFDM, combinations of $M = 1024$ with $L = 2$, $M = 512$ with $L = 3$ and $M = 256$ with $L = 4$ are utilized, of which the spectral efficiency is respectively 3.75, 3.9375 and 3.75 bits/channel use based on (21). For AAO-OFDM, $M_1 = 512$ with $M_2 = 1024$ is employed, of which the spectral efficiency is $\Upsilon_{\text{AAO}} = 3.75$ bits/channel use according to (22). It can be seen that eU- and LACO-OFDM have the similar BER performance with the same layer number and constellation size, in which the spectral efficiencies of the both schemes are the same.

Consider comparing schemes with the same spectral efficiency and number of layers. Fig. 9 indicates that ALACO- with $M = 256$ and $L = 2$ has the best BER performance compared to eU- with $M = 1024$ and $L = 2$, LACO- with $M = 1024$ and $L = 2$ and AAO-OFDM with $M_1 = 512$ and $M_2 = 1024$ at the same spectral efficiency of 3.75 bits/channel use. When the BER approaches

10^{-6}, ALACO-OFDM achieves about 1.3, 1.4 and 0.8 dB performance gains over eU-, LACO- and AAO-OFDM, respectively. This is because ALACO-OFDM can employ smaller constellation size M to achieve the same spectral efficiency compared to the other three schemes.

Considering only the spectral efficiency, from Sec. III-A, increasing L improves the spectral efficiency of ALACO-, eU- and LACO-OFDM. Notice that ALACO- with $M = 256$ and $L = 2$ has about 0.2 dB gain over eU- and LACO-OFDM with $M = 256$ and $L = 4$ at BER$= 10^{-6}$. The spectral efficiencies of all schemes noted are the same, however, ALACO-OFDM is able to provide a gain while operating with less complexity and latency (i.e., smaller L). Similarly at a higher spectral efficiency, ALACO-OFDM with $M = 256$ and $L = 4$ achieves about 0.2 dB gain at BER$= 10^{-6}$ compared to eU- and LACO-OFDM with $M = 512$ and $L = 3$ at the spectral efficiency of 3.9375 bits/channel use. Thus, ALACO-OFDM provides higher spectral efficiencies over earlier approaches while retaining the power efficiency of ACO-OFDM schemes.

B. Probability Density Function

In this section, the PDF of ALACO-OFDM time-domain signal for different number of layers is investigated. In ALACO-OFDM, L layers of ACO-OFDM time-domain signal are independent. Although first layer ACO-OFDM signal carries sign bits of AVO-OFDM signal, the both are independent [3]. Hence, the PDF of ALACO-OFDM can be calculated by convolving the PDFs of L layers of ACO-OFDM and the PDF of AVO-OFDM. Then the PDF of ALACO-OFDM is given by

$$f_{\mathrm{AL}}^{(L)}(\xi) = f_1(\xi) \otimes \ldots \otimes f_L(\xi) \otimes f_v(\xi) \tag{71}$$

where $\otimes$ denotes convolution operation and $f_l(\xi)$ and $f_v(\xi)$ are given by (40) and (42).

The simulated and theoretical PDF of ALACO-OFDM are shown in Fig. 10, in which the total optical power is set to unity and $\alpha = \sqrt{2}$. For the simulated PDF, $N = 1024$ subcarriers and 16-QAM are utilized. It can be seen the simulated and theoretical PDF of ALACO-OFDM are aligned well.

C. PAPR Comparison

In this section, the PAPR of ALACO-OFDM is compared versus its counterparts. Define the PAPR of a discrete time-domain signal z_n as [31]

$$\mathrm{PAPR} = \frac{\max\limits_{0 \le n \le N-1} z_n^2}{\mathrm{E}\{z_n^2\}}. \tag{72}$$

The complementary cumulative distribution function (CCDF) of PAPR is defined as

$$\mathrm{CCDF}(\gamma) = 1 - \Pr\{\mathrm{PAPR} \le \gamma\} \tag{73}$$

where $\Pr\{\Psi\}$ denotes the probability of an event Ψ.

Following the method calculating the CCDF of LACO-OFDM in [18], the CCDF(γ) can be well approximated using its PDF as

$$\mathrm{CCDF}(\gamma) \approx 1 - \left(2 \int_{-\infty}^{\sqrt{\gamma \mathrm{E}\{z_n^2\}}} f_{\mathrm{AL}}^{(L)}(\xi) d\xi - 1\right)^{N/2}. \tag{74}$$

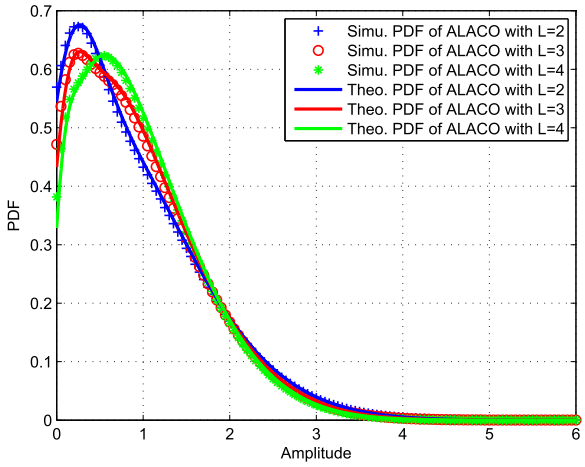

Fig. 10. Simulated and theoretical PDF of ALACO-OFDM with $L = 2$, 3, and 4 ('Simu.' and 'Theo.' denote 'Simulated' and 'Theoretical', respectively).

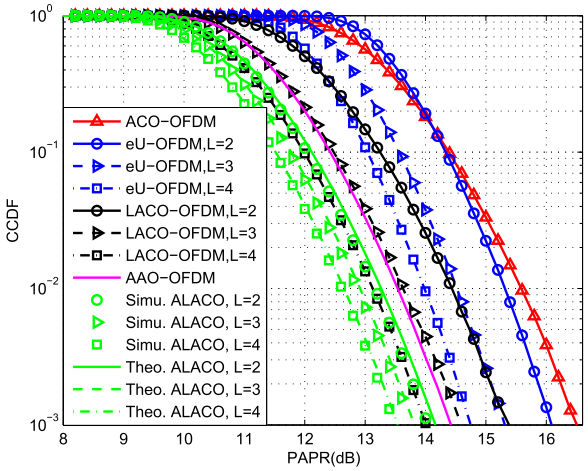

Fig. 11. PAPR comparison between ALACO-OFDM and its counterparts with $N = 1024$ subcarriers ($\alpha = \sqrt{2}$ is used for ALACO, LACO-, and eU-OFDM).

The CCDF of PAPR in ALACO- with different total layer number L is analyzed and compared to ACO-, eU-, LACO- and AAO-OFDM as shown in Fig. 11 for $N = 1024$. It can be seen the theoretical CCDFs of ALACO-OFDM approximated by (74) agree well with the simulated results for different number of layers. It is evident that ACO-OFDM has the worst PAPR performance. For eU-, LACO- and ALACO-OFDM, the PAPR performance becomes better as the total layer number L increases from 2 to 4. This trend was also noticed in earlier work [18]. When CCDF $= 10^{-3}$, the PAPR of ALACO- with $L = 2$ is about 0.4 dB, 1.3 dB, 2.1 dB and 2.5 dB smaller compared to AAO-, LACO- with $L = 2$, eU- with $L = 2$ and ACO-OFDM, respectively. This is because for the same peak value, the average electrical power of ALACO-OFDM is bigger, which leads to a smaller PAPR according to (72). When CCDF approaches 10^{-3}, the PAPR of ALACO- with $L = 4$ is about 0.9 dB, 0.5 dB, 1.3 dB and 3.1 dB smaller compared to AAO-, LACO- with $L = 4$, eU- with $L = 4$ and ACO-OFDM, respectively. The analysis and comparison between ALACO-OFDM and its counterparts suggests that ALACO-OFDM, with its lower PAPR, may be less sensitive to LED nonlinearity.

VI. Conclusion

In this paper, ALACO-OFDM is proposed to enhance the spectral efficiency for IM/DD OFDM communications while retaining power efficiency. Signal analysis indicates the spectral efficiency gap between ALACO- and DCO-OFDM can be made negligible even with a small number of layers. Notice that ALACO-OFDM is a generalization of AAO-OFDM and has a spectral efficiency that is $\frac{\log_2 M-2}{2^{L+1}}$ bits/channel use larger than eU- or LACO-OFDM with the same layer number L. Two optical power allocation schemes are discussed over the layers of ALACO-OFDM with the objective of optimizing uncoded transmission performance and the achievable information rate respectively. ALACO-OFDM with optical power allocation factor $\alpha = 2$ achieves optimal rate while the optimal uncoded BER performance is achieved when $\alpha = \sqrt{2}$. A theoretical bound on the uncoded BER of ALACO-OFDM is also derived, which matches the simulated BER in high SNR regime. The information rate analysis also indicates ALACO- can achieve higher rate with even smaller number of layers than LACO-OFDM. In addition, ALACO- has smaller PAPR compared to eU-, LACO- and AAO-OFDM, which suggests better performance on nonlinear LED channels. Complexity analysis indicates the computational complexity of ALACO-OFDM is on the same order at LACO- and eU-OFDM while realizing performance gains. Monte Carlo simulation of BER performance is analyzed and compared, from which it can be concluded that ALACO- has the best BER performance over layered ACO-OFDM approaches with the same spectral efficiency while using a smaller number of layers.

This paper focuses on transceiver design for ALACO-OFDM and shows its advantage with a smaller number of layers over its counterparts operating at a given spectral efficiency. Future investigation include integrating ALACO-OFDM with error control coding, PAPR suppressing approaches, specially designed low-complex FFTs/IFFTs for ACO- and AVO-OFDM as well as the use of alternate transforms such as the Harley transform.

Appendix A
Proof of the Achievable Information Rate of the Absolute-Value Gaussian Channel

Given $y = |x|$ and $x \sim N(0, \sigma_x^2)$, y follows a truncated Gaussian distribution. Given y and w are independent, $z = y + w$ has PDF

$$f_z(z) = \int_{-\infty}^{\infty} f_w(w) f_y(z-w) dw = 2\left(1 - Q\left(\frac{z\sigma_x}{\sigma_w \sigma}\right)\right) \frac{1}{\sqrt{2\pi}\sigma} \exp\left\{-\frac{z^2}{2\sigma^2}\right\} \quad (75)$$

where $\sigma \triangleq \sqrt{\sigma_w^2 + \sigma_x^2}$ and $Q(x) = \int_x^{\infty} \frac{1}{\sqrt{2\pi}} \exp\{-\frac{t^2}{2}\} dt$. The differential entropy of z is thus

$$h(z) = -\int_{-\infty}^{\infty} f_z(z) \log f_z(z) dz = \frac{1}{2} \log 2\pi e\sigma^2 - (1-D) \quad (76)$$

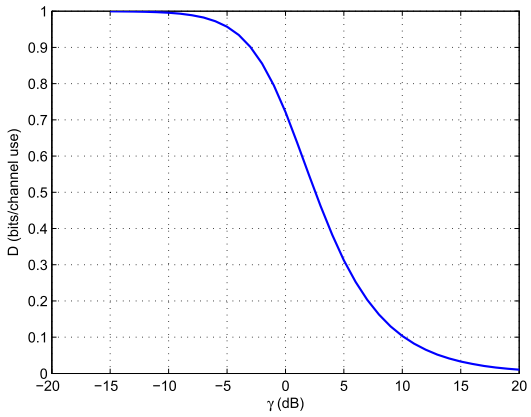

Fig. 12. D as a function of γ.

where

$$\begin{aligned} D &= -\int_{-\infty}^{\infty} f_z(z) \log\left(1 - Q(\frac{z\sigma_x}{\sigma_w\sigma})\right) dz \\ &\overset{(a)}{=} -2\int_{-\infty}^{\infty} (1 - Q(t\gamma)) \log(1 - Q(t\gamma)) \frac{1}{\sqrt{2\pi}} \exp\left\{-\frac{t^2}{2}\right\} dt \\ &\overset{(b)}{=} -2\int_{0}^{\infty} (1 - Q(t\gamma)) \log(1 - Q(t\gamma)) \frac{1}{\sqrt{2\pi}} \exp\left\{-\frac{t^2}{2}\right\} dt \\ &\quad -2\int_{0}^{\infty} Q(t\gamma) \log Q(t\gamma) \frac{1}{\sqrt{2\pi}} \exp\left\{-\frac{t^2}{2}\right\} dt \\ &\overset{(c)}{=} 2\int_{0}^{\infty} \mathcal{H}(Q(t\gamma)) \frac{1}{\sqrt{2\pi}} \exp\left\{-\frac{t^2}{2}\right\} dt \end{aligned} \quad (77)$$

where $\mathcal{H}(p)$ is the entropy of a Bernoulli random variable with probability p. Step (a) is based on integration by substitution $t = z/\sigma_w\sqrt{\gamma^2+1}$ while step (b) is based on $1 - Q(-t\gamma) = Q(t\gamma)$ and

$$\int_{-\infty}^{0} (1 - Q(t\gamma)) \log(1 - Q(t\gamma)) \frac{1}{\sqrt{2\pi}} \exp\left\{-\frac{t^2}{2}\right\} dt \overset{u=-t}{=} \int_{0}^{\infty} Q(u\gamma) \log Q(u\gamma) \frac{1}{\sqrt{2\pi}} \exp\left\{-\frac{u^2}{2}\right\} du. \quad (78)$$

Step (c) arises from the definition of the entropy of a Bernoulli random variable.

Hence, the capacity of this absolute-value Gaussian channel is found by substituting $h(z)$ and $h(w) = \frac{1}{2}\log 2\pi e\sigma_w^2$ into

$$C_{\text{v}} = I(z;y) = h(z) - h(z|y) = h(z) - h(w) \quad (79)$$

to give

$$C_{\text{v}} = \frac{1}{2}\log\left(1 + \frac{\sigma_x^2}{\sigma_w^2}\right) - (1-D) \text{ bits/channel use.} \quad (80)$$

Note that $0 < \mathcal{H}(Q(t\gamma)) \leq 1$. Hence, we have

$$0 < D \leq 2\int_0^{\infty} \frac{1}{\sqrt{2\pi}} \exp\left\{-\frac{t^2}{2}\right\} dt = 1 \quad (81)$$

where the upper bound can be achieved when $\gamma = 0$.

For $t > 0$, if $0 \leq \gamma_1 < \gamma_2$ then $0 < Q(t\gamma_2) < Q(t\gamma_1) \leq 1/2$ and thus $\mathcal{H}(Q(t\gamma_1)) > \mathcal{H}(Q(t\gamma_2))$. Hence, we have

$$D(\gamma_1) - D(\gamma_2) = 2\int_0^{\infty} (\mathcal{H}(Q(t\gamma_1)) - \mathcal{H}(Q(t\gamma_2))) \frac{1}{\sqrt{2\pi}} \exp\left\{-\frac{t^2}{2}\right\} dt > 0 \quad (82)$$

which indicates $D(\gamma)$ is monotonically decreasing in γ and $D \longrightarrow 0$ as $\gamma \longrightarrow \infty$. Fig. 12 shows D for different values of γ.

REFERENCES

[1] L. Hanzo, H. Haas, S. Imre, D. O'Brien, M. Rupp, and L. Gyongyosi, "Wireless myths, realities, and futures: From 3G/4G to optical and quantum wireless," *Proc. IEEE*, vol. 100, no. Special Centennial Issue, pp. 1853–1888, May 2012.

[2] J. M. Kahn and J. R. Barry, "Wireless infrared communications," *Proc. IEEE*, vol. 85, no. 2, pp. 265–298, Feb. 1997.

[3] R. Bai, Q. Wang, and Z. Wang, "Asymmetrically clipped absolute value optical OFDM for intensity-modulated direct-detection systems," *J. Lightw. Technol.*, vol. 35, no. 17, pp. 3680–3691, Sep. 1, 2017.

[4] J. Armstrong, "OFDM for optical communications," *J. Lightw. Technol.*, vol. 27, no. 3, pp. 189–204, Feb. 1, 2009.

[5] S. D. Dissanayake and J. Armstrong, "Comparison of ACO-OFDM, DCO-OFDM and ADO-OFDM in IM/DD systems," *J. Lightw. Technol.*, vol. 31, no. 7, pp. 1063–1072, Apr. 2013.

[6] D. Tsonev and H. Haas, "Avoiding spectral efficiency loss in unipolar OFDM for optical wireless communication," in *Proc. IEEE Int. Conf. Commun. (ICC)*, Sydney, NSW, Australia, Jun. 2014, pp. 3336–3341.

[7] L. Chen, B. Krongold, and J. Evans, "Successive decoding of anti-periodic OFDM signals in IM/DD optical channel," in *Proc. IEEE Int. Conf. Commun.*, Cape Town, South Africa, May 2010, pp. 1–6.

[8] H. Elgala and T. D. C. Little, "SEE-OFDM: Spectral and energy efficient OFDM for optical IM/DD systems," in *Proc. IEEE 25th Annu. Int. Symp. Pers., Indoor, Mobile Radio Commun. (PIMRC)*, Washington, DC, USA, Sep. 2014, pp. 851–855.

[9] Q. Wang, C. Qian, X. Guo, Z. Wang, D. G. Cunningham, and I. H. White, "Layered ACO-OFDM for intensity-modulated direct-detection optical wireless transmission," *Opt. Express*, vol. 23, no. 9, pp. 12382–12393, May 2015.

[10] M. S. Islim, D. Tsonev, and H. Haas, "On the superposition modulation for OFDM-based optical wireless communication," in *Proc. IEEE Global Conf. Signal Inf. Process. (GlobalSIP)*, Orlando, FL, Dec. 2015, pp. 1022–1026.

[11] Q. Wang *et al.*, "Hardware-efficient signal generation of layered/enhanced ACO-OFDM for short-haul fiber-optic links," *Opt. Express*, vol. 25, no. 12, pp. 13359–13371, Jun. 2017.

[12] R. Bai and S. Hranilovic, "Absolute value layered ACO-OFDM for intensity-modulated optical wireless channels," in *Proc. IEEE Int. Conf. Commun. (ICC)*, Shanghai, China, May 2019, pp. 1–6.

[13] B. Porat, *A Course in Digital Signal Processing*. New York, NY, USA: Wiley, 1997.

[14] R. Bai and S. Hranilovic, "Layered antisymmetry-constructed clipped optical OFDM for IM/DD systems," in *Proc. IEEE Global Commun. Conf. (GLOBECOM)*, Waikoloa, HI, USA, Dec. 2019, pp. 1–6.

[15] X. Li, R. Mardling, and J. Armstrong, "Channel capacity of IM/DD optical communication systems and of ACO-OFDM," in *Proc. IEEE Int. Conf. Commun.*, Glasgow, U.K., 2007, pp. 2128–2133.

[16] Y. Sun, F. Yang, and J. Gao, "Novel dimmable visible light communication approach based on hybrid LACO-OFDM," *J. Lightw. Technol.*, vol. 36, no. 20, pp. 4942–4951, Oct. 15, 2018.

[17] L. Chen, B. Krongold, and J. Evans, "Performance analysis for optical OFDM transmission in short-range IM/DD systems," *J. Lightw. Technol.*, vol. 30, no. 7, pp. 974–983, Apr. 2012.

[18] X. Zhang, Q. Wang, R. Zhang, S. Chen, and L. Hanzo, "Performance analysis of layered ACO-OFDM," *IEEE Access*, vol. 5, pp. 18366–18381, 2017.

[19] X. Zhang, Z. Babar, R. Zhang, S. Chen, and L. Hanzo, "Multi-class coded layered asymmetrically clipped optical OFDM," *IEEE Trans. Commun.*, vol. 67, no. 1, pp. 578–589, Jan. 2019.

[20] Y. Sun, F. Yang, and L. Cheng, "An overview of OFDM-based visible light communication systems from the perspective of energy efficiency versus spectral efficiency," *IEEE Access*, vol. 6, p. 60824–60833, 2018.

[21] R. Bai, Z. Wang, R. Jiang, and J. Cheng, "Interleaved DFT-spread Layered/Enhanced ACO-OFDM for intensity-modulated direct-detection systems," *J. Lightw. Technol.*, vol. 36, no. 20, pp. 4713–4722, Oct. 15, 2018.

[22] C. E. Shannon, "A mathematical theory of communication," *Bell Syst. Tech. J.*, vol. 27, no. 3, pp. 379–423, Jul./Oct. 1948.

[23] J. Zhou and W. Zhang, "A comparative study of unipolar OFDM schemes in Gaussian optical intensity channel," *IEEE Trans. Commun.*, vol. 66, no. 4, pp. 1549–1564, Apr. 2018.

[24] S. Mazahir, A. Chaaban, H. Elgala, and M.-S. Alouini, "Achievable rates of multi-carrier modulation schemes for bandlimited IM/DD systems," *IEEE Trans. Wireless Commun.*, vol. 18, no. 3, pp. 1957–1973, Mar. 2019.

[25] J. Grubor, S. Randel, K.-D. Langer, and J. W. Walewski, "Broadband information broadcasting using LED-based interior lighting," *J. Lightw. Technol.*, vol. 26, no. 24, pp. 3883–3892, Dec. 15, 2008.

[26] M. S. A. Mossaad, S. Hranilovic, and L. Lampe, "Visible light communications using OFDM and multiple LEDs," *IEEE Trans. Commun.*, vol. 63, no. 11, pp. 4304–4313, Nov. 2015.

[27] A. A. Farid and S. Hranilovic, "Capacity bounds for wireless optical intensity channels with Gaussian noise," *IEEE Trans. Inf. Theory*, vol. 56, no. 12, pp. 6066–6077, Dec. 2010.

[28] S. Hranilovic and F. R. Kschischang, "Capacity bounds for power-and band-limited optical intensity channels corrupted by Gaussian noise," *IEEE Trans. Inf. Theory*, vol. 50, no. 5, pp. 784–795, May 2004.

[29] A. Lapidoth, S. M. Moser, and M. A. Wigger, "On the capacity of free-space optical intensity channels," *IEEE Trans. Inf. Theory*, vol. 55, no. 10, pp. 4449–4461, Oct. 2009.

[30] D. Tsonev, S. Videv, and H. Haas, "Unlocking spectral efficiency in intensity modulation and direct detection systems," *IEEE J. Sel. Areas Commun.*, vol. 33, no. 9, pp. 1758–1770, Sep. 2015.

[31] J. Wang, Y. Xu, X. Ling, R. Zhang, Z. Ding, and C. Zhao, "PAPR analysis for OFDM visible light communication," *Opt. Express*, vol. 24, no. 24, pp. 27457–27474, Nov. 2016.

Ruowen Bai (Graduate Student Member, IEEE) received the B.E. degree from Nankai University in 2015 and the M.E. degree from Tsinghua University, China, in 2018. He is currently pursuing the Ph.D. degree with McMaster University. His research interests include modulation and signal processing for wireless communications and visible light communications.

Steve Hranilovic (Senior Member, IEEE) received the B.A.Sc. degree (Hons.) in electrical engineering from the University of Waterloo, Canada, in 1997, and the M.A.Sc. and Ph.D. degrees in electrical engineering from the University of Toronto, Canada, in 1999 and 2003, respectively.

From 2010 to 2011, he spent his research leave as a Senior Member and a Technical Staff at the Advanced Technology for Research in Motion, Waterloo, Canada. He is currently a Professor with the Department of Electrical and Computer Engineering, McMaster University, Hamilton, ON, Canada, where he serves as the Associate Dean (Academic). His research interests include free-space and optical wireless communications, digital communication algorithms, and electronic and photonic implementation of coding and communication algorithms. He is the author of the book *Wireless Optical Communication Systems* (New York: Springer, 2004).

Dr. Hranilovic was awarded the Government of Ontario Early Researcher Award in 2006. He has served as an Associate Editor for *Journal of Optical Communications and Networking* and an Editor for IEEE TRANSACTIONS ON COMMUNICATIONS in the area of optical wireless communications. He is a licensed Professional Engineer in the Province of Ontario.